International Journal of Mechanical System Dynamics

WILEY

IJMSD International Journal of Mechanical System Dynamics Open Access

RESEARCH ARTICLE OPEN ACCESS

Detecting Loosening of Bolt-Flanged Pipe Using Smoothed Pseudo Wigner–Ville Distribution: Digital Twin-Based Approach Using Convolution Neural Networks

Milad Shabani Yousefabad[1] | Behzad Totakhaneh Bonab[1] | Morteza Homayoun Sadeghi[1] | Mir Mohammad Ettefagh[1] | Mohammad Reza Chalak Qazani[2,3]

[1]Faculty of Mechanical Engineering, University of Tabriz, Tabriz, Iran | [2]College of Science and Engineering, James Cook University, Townsville, Queensland, Australia | [3]Faclty of Computing and Information Technology, Sohar University, Sohar, Oman

Correspondence: Mohammad Reza Chalak Qazani (mohamadreza.chalakqazani@jcu.edu.au)

Received: 4 August 2025 | **Revised:** 26 April 2026 | **Accepted:** 1 May 2026

Keywords: convolution neural networks | finite element modeling | Haar filter bank | smoothed pseudo Wigner–Ville distribution

ABSTRACT

In this paper, an integrated digital twin-based fault-diagnosis framework is proposed to detect bolt loosening in flanged pipe connections. The approach combines finite element-based numerical modeling, experimental modal analysis, and advanced signal processing-assisted deep learning to achieve reliable loosening detection under operational excitations. First, a finite element model of the bolted flange pipe is developed and updated using experimentally identified natural frequencies to establish a validated digital twin. The dynamic responses of healthy and loosened bolt conditions are then simulated and experimentally measured. To extract fault-sensitive features, the vibration signals are decomposed using a Haar filter bank, followed by transformation into the time–frequency domain using the Smoothed Pseudo Wigner– Ville distribution (SPWVD). The resulting time–frequency representations are subsequently used to train a convolutional neural network (CNN). A key contribution of this study lies in the hybrid digital twin learning strategy, in which CNN training is performed using numerical data and healthy experimental data. At the same time, fault classification is conducted under experimental loosening conditions. The results demonstrate that the proposed framework effectively captures bolt loosening signatures and provides a practical, physics-consistent solution for condition monitoring of bolted flange connections.

1 | Introduction

Nowadays, monitoring mechanical systems and structures is particularly important, as their failure or defects can cause irreparable human and financial damage. Therefore, to prevent failures and structural breakdowns, they need to be controlled and monitored. Monitoring requires unique indicators for fault detection, which, given the diverse applications of mechanical systems across industries, makes the monitoring process more challenging. Structures are connected by various means, including welding and bolting, with bolted connections being among the most prominent. These connections are exposed to time-varying environmental actions, including seismic excitations, wind loading, and thermal fluctuations, which may progressively lead to degradation and loosening of the connections. For this reason, to prevent their failure, they need to be monitored. Pipe flange connections are another prominent example of flanged connections, widely used in gas transmission lines and refineries, and can experience leakage due to bolt loosening under these environmental factors. Thananjayan et al. [1]

presented a deep learning approach using convolutional neural networks trained on photoelastic fringe patterns generated via the quadtree-based scaled boundary finite element method to accurately identify and characterize circular flaws and cracks in structures, achieving prediction accuracies of up to 99%. Dessena et al. [2] introduced NExT-LF, a robust and noise-resistant method combining the Natural Excitation Technique with the Loewner Framework for output-only modal parameter identification, validated through numerical and experimental studies, including the first OMA application on the Sheraton Universal Hotel. Khalid et al. [3] introduced an efficient triangular inverse shell element based on discrete Kirchhoff assumptions within the iFEM framework, enabling accurate displacement reconstruction with fewer sensors for real-time structural health monitoring of thin shell structures, and demonstrating superior performance over FSDT-based elements through extensive validation and damage assessment.

The dynamic behavior of bolts has long been a significant research topic. He and Zhu [4] presented a finite element model for L-shaped beam connections and studied the effects of bolt tightness and bolt mass on assembled structures. Additionally, Bograd et al. [5] performed dynamic modeling of mechanical connections using various methods, examining the results for each approach. Furthermore, Zerres and Guérout [6] used the Taylor Forge method for bolted flange connections and demonstrated that the proposed method can assess the acceptability of bolted flange connections under service conditions. Xing et al. [7] proposed modeling multi-plate structures using Kirchhoff's plate theory, employing Chebyshev orthogonal functions as admissible functions to derive the governing equations. They also used the Rayleigh–Ritz method for free vibrations and the Newmark-beta method for forced vibrations, with experimental tests performed to compare the results. Zhao et al. [8] applied a non-destructive testing method for bolted connections to identify the preload force of a bolt using both contact and non-contact identification methods. They also discussed the advantages and disadvantages of these methods in diagnosing bolted connections. In addition to the mentioned modeling, Zheng et al. [9] studied the shear behavior of bolted connections, the impact of joint surface wear on reducing the internal friction angle, and the relationship between bolt loosening and deformation. Ouyang et al. [10] studied macro- and micro-slip phenomena in flange connections, analyzing damping behavior from linear viscous to nonlinear frictional types in hysteresis loops. Furthermore, Tang et al. [11] discussed the effects of the number of connection bolts and their tightness on modal parameters, including natural frequencies, using Sander's shell theory. Finally, Yang et al. [12] discussed finite element modeling and the vibration characteristics of a shaft-disk-drum rotor system with bolted connections.

Given the nonlinear behavior of the mentioned connections, researchers have not only modeled and studied their linear behavior but also explored their nonlinear behavior. Jamia et al. [13] presented an equivalent model for nonlinear bolted flange connections and studied the micro-slip behavior in hysteresis loops, indicating nonlinear response. Jalali et al. [14] demonstrated that by identifying the nonlinear parameters of a bolt-edge connection using force mapping, the complex phenomenon of energy dissipation can be revealed through the proposed model. Lacayo et al. [15] modeled a Brake–Reuß beam with bolted connections, applying both time-domain and frequency-domain approaches. They first updated the model for both approaches and then predicted the nonlinear dynamic response for the second and third modes. Additionally, bolted flange connections have numerous applications in aircraft, even in their engines. For this reason, Schwingshackl et al. [16] developed a model to model and validate the nonlinear behavior of bolted flange connections. The outcome of their research can be summarized in two perspectives: the distribution of steady–state stress in the connections and the distribution of nonlinear element numbers. In addition to studies on micro- and macro-slip, Gaul and Lenz [17] conducted finite-element modeling of contact points in mechanisms, including bolted connections. Estakhraji et al. [18] used a semi-static modal analysis method to determine damping ratios and natural frequencies in bolted structures. They compared their results with those obtained under different preload conditions. Furthermore, Liu et al. [19] presented a nonlinear finite element analysis model for bolted thin plates, studying the resonance frequency and the frequency response amplitude of the bolted thin plate. Also, Tan et al. [20] examined the hysteresis behavior and parameters of bolted connections by presenting an analytical model of a bolt. Then they analyzed the mechanism of the bolt thread connection under non-parallel bearings. Ibrahim and Pettit [21] discussed uncertainties and dynamic issues in bolted connections, with key findings on energy dissipation in connections and the identification of both linear and nonlinear dynamic properties of connections. On the other hand, in addition to modeling and studying the behavior of bolted flange connections, monitoring them to prevent defects is also valuable among researchers. Argatov and Sevostianov [22] proposed electrical resistance as a health-monitoring parameter for bolted-connection structures. Additionally, Nichols et al. [23] focused on detecting the loosening of a composite-to-metal screw connection under high-temperature fluctuations. Finally, Ritdumrongkul and Fujino [24] studied the identification of loosening location and amount in multi-bolt connections using PZT sensor-actuators.

As previously mentioned, pipe flange connections are a prominent example of bolted flange connections, and their modeling and behavior have been the subject of ongoing research. Luan et al. [25] proposed a simplified nonlinear dynamic model for a pipe flange connection with a semi-linear spring, discussing the transverse vibration frequencies and the beam vibrations that lead to coupled vibrations. Additionally, Shi and Zhang [26] initially studied the elastostatic properties of the pipe flange using finite element analysis, discussing the relationships between vibrational properties and preloading. Moreover, pipe flanges can be subjected to tensile, torsional, or bending loads, which is why Wu et al. [27] studied the nonlinear deformation behavior of pipe flanges under bending, torsion, and tensile loads using finite element analysis. Furthermore, Li et al. [28] experimentally and theoretically studied the free and forced vibrations of composite cylindrical–cylindrical shells with partial bolt loosening connections. In their study, the theoretical model was based on primary and secondary hypotheses regarding spring connections with reduced tightness at different bolt loosening positions, and they thoroughly described the sources of error. Another goal of pipe flange connection modeling is to model its sealing by gaskets using finite element methods, which has been fully discussed in [29, 30]. Fault detection in pipe flange connections is as important as detecting faults in bolted connections. Among the studies conducted, Bonab et al. [31] proposed a method for diagnosing pipe flange connection faults by modeling the pipe flange parametrically and using a bolt-loosening index based on the Mahalanobis distance. Additionally, frequency changes have long been considered an indicative parameter for fault detection. In this regard, He and Zhu [32] used a finite element model to study loosening of pipe flange connections by analyzing changes in frequency. Another method for detecting bolt loosening in flange connections is the empirical mode decomposition index, studied by Razi et al. [33] using a finite element model.

Today, various methods are used for monitoring mechanical systems and structures. As artificial intelligence advances across various fields, researchers and engineers use it as a tool for fault diagnosis. Deep learning, a subset of artificial intelligence, is widely used today for fault diagnosis. Cha et al. [34] discussed various fault diagnosis methods performed using deep learning. In the past, to diagnose faults in mechanical systems or structures, they were intentionally damaged and used for training networks, which is not feasible. However, today, with the computer modeling of these structures and the design of appropriate neural networks, a new theory called digital twin is applied. The computer model here is not just an accurate representation of the experimental model; it must also exhibit fault-sensitivity. Signal processing methods are then used to extract fault features, which, along with the results of computer simulations, are used to train the proposed neural networks and are eventually tested against experimental model results. Among related studies, the fault diagnosis of a floating wind turbine structure under different conditions has been addressed by Mousavi et al. [35], who introduced their digital twin using computer modeling and deep neural networks and then performed fault diagnosis. Additionally, using finite element modeling and deep neural networks in [36, 37], they addressed fault diagnosis of a jacket platform under various fault scenarios. Structural health monitoring of bridges to prevent catastrophic accidents has always been valuable for engineers. For this reason, researchers have applied digital twin technology to monitor bridges, as discussed in [38–40]. Chen et al. [41] further explored structural damage assessment of PC beam bridges through digital twin model updating, using finite element modeling. Beyond bridges, the digital twin of cable-stay structures has been studied by Shi et al. [42] using finite-element modeling. Moreover, Jayasinghe et al. [43] presented a finite element model and neural networks specifically for a digital twin of a coastal structure, and the same approach has been discussed for assembled aircraft systems and autonomous ships in [44, 45]. Mousavi et al. [46] used finite element models and dynamic response for fault diagnosis of beams, followed by using deep neural networks. Furthermore, Hu et al. [47] proposed a digital twin for diagnosing active magnetic bearings, and Gong et al. [48] also applied the digital twin method for bearing fault diagnosis. Finally, one of the most relevant studies in the digital twin field is Wang et al.'s pipeline study, which focuses on diagnosing fatigue-induced cracks [49].

The initial decomposition of measured responses into multiscale components is a prerequisite for isolating fault-related dynamics. Filter banks based on Haar functions have gained popularity due to their strict mathematical orthogonality and simple implementation, which yield compact feature sets for subsequent learning stages.

1. Wind and Structural Applications: Dunyak et al. [50] employed Haar-based transformations to identify coherent gust patterns within turbulent wind data, thereby distinguishing them from random fluctuations that may mask structural responses. Similarly, Kim et al. [51, 52] utilized Haar and related wavelet models with low-order mode shapes to infer stiffness reductions and localize potential damage in beam- and plate-type elements; their formulations explicitly addressed modal selection and parameter-identification challenges.
2. Machinery Fault Detection: Li et al. [53] highlighted the diagnostic capacity of the Haar-based Continuous Wavelet Transform (HCWT) for rotary systems, emphasizing its balanced time–frequency localization and superior

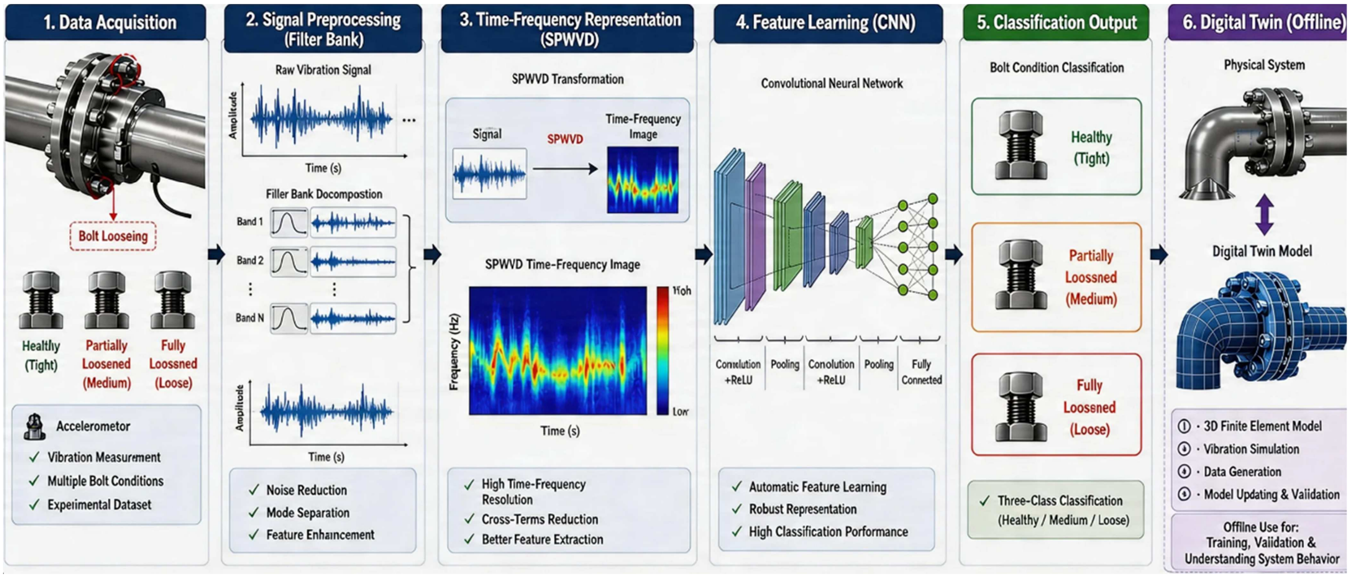

FIGURE 1 | Flowchart of the proposed method.

low-pass filtering over the more conventional Morlet function. Subsequent studies expanded this concept to interpret the energy contribution of wavelet coefficients as indicators of damage severity. Nair and Kiremidjian [54] developed an analytical expression linking coefficient energy at higher scales with system parameters and loading states, while Kesavan and Kiremidjian [55] integrated wavelet-based preprocessing with cluster-based classification schemes for automated damage recognition.

3. Sensor-Level and Component Diagnostics: Jayakumar and Thangavel [56] demonstrated that Haar decomposition of vibration signals enables differentiation between healthy and faulty induction motors, particularly for bearing degradation. Bhattacharya et al. [57] further applied discrete Haar transforms to high-frequency data from PZT sensors to quantify flaws on the order of 100 μm.
4. Complex and Multiscale Systems: Expanding toward large-scale machinery, Monieta [58] combined wavelet-based time–frequency processing with learning techniques for marine diesel injectors, showing reliability improvements compared to conventional vibration indices. Recent AI-oriented studies integrate Haar features directly within neural networks: Zhang et al. [59] designed the Dual-Encoder Crack Segmentation Network (DECS-Net) using multi-resolution attention to analyze image-based cracks, and Hang et al. [60] embedded Haar-wavelet attention into the MIP-YOLO architecture for autonomous defect detection in turbine blades, enhancing recognition accuracy and operational efficiency.

In data-driven structural health monitoring, selecting features that are strongly influenced by damage mechanisms is essential for designing effective learning models. Approaches differ in how they transform vibration responses into discriminative representations, among which time–frequency analyses have shown value. The Wigner–Ville framework, as a quadratic time–frequency technique, provides high-resolution energy localization that assists neural networks in fault pattern recognition far more than conventional transforms. Earlier studies applied this principle to many mechanical systems: for instance, diesel valve monitoring in railway engines (Chengdong et al. [61]), gear defect characterization via energy density functions (Loutridis [62]), and fault classification in composite structures through convolutional architectures (Carvalho Monson et al. [63]). Similar formulations have also been extended to numerous devices from scooter motors and rotating beams to bridge and engine systems using manifold pressure or vibration signals [64–67]. Building upon these developments, recent studies employ the Smoothed Pseudo Wigner–Ville variant, in which temporal smoothing suppresses cross-term artefacts and improves fault localization accuracy [68–71]. Yousefabad et al. utilized the Smoothed Pseudo Wigner–Ville Distribution to map vibration responses of offshore monopile systems into detailed time–frequency domains, allowing damage-related characteristics to be effectively highlighted under randomly varying environmental loads [72].

The main objective of this paper is to diagnose faults in flanged pipe connections using digital twin technology. Initially, a finite element model of the flanged pipe with bolted connections is created, and the system natural frequencies are extracted. It is important to note that the primary goal is not to create a complex computer model and to extract a precise dynamic response, as in the experimental model. Instead, the focus is on modeling to extract fault-sensitive features. To achieve this,

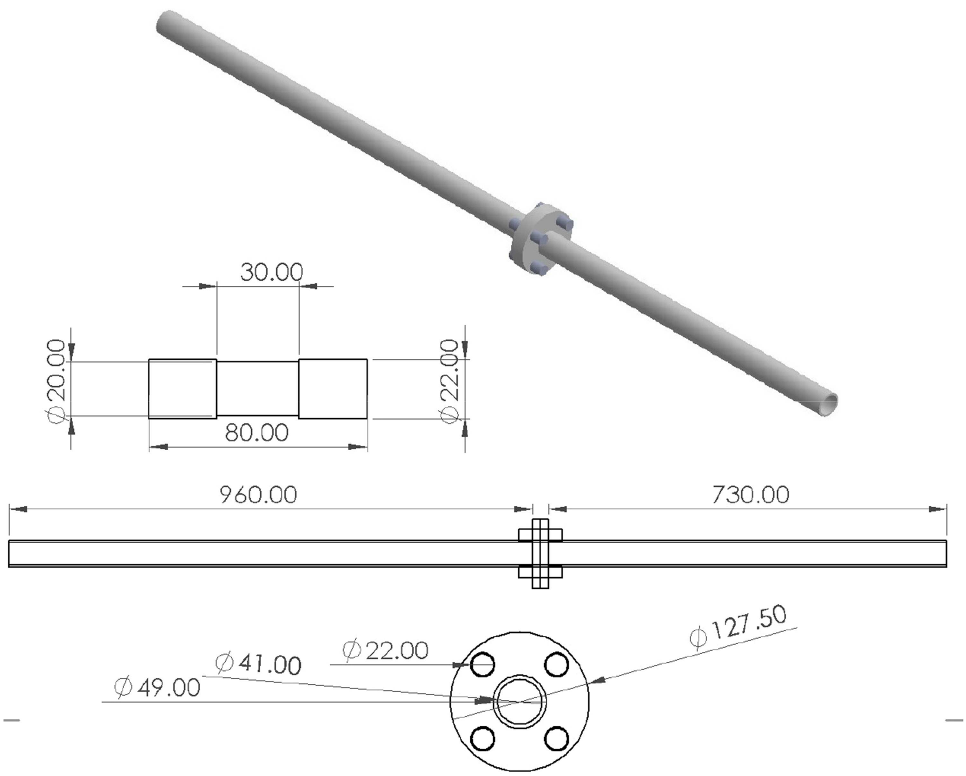

FIGURE 2 | Geometry of the flanged pipe (dimensions in millimeters).

after developing an appropriate computer model, a flanged pipe with identical dimensions to the computer model is prepared and subjected to experimental modal analysis. Data collection is performed using a roving accelerometer and impulse hammer excitation, and experimental modal analysis methods are employed to obtain natural frequencies. The natural frequencies obtained from the experimental model serve as a suitable source for updating the parameters of the computer model. After verifying the accuracy of the computer model parameters, specialized software generates a white noise signal. The flanged pipe is then excited via a shaker, and the finite element model is also excited, and the dynamic responses are recorded. In the next step, bolt loosening is defined as a system fault, and the computer model is simulated in three states: fully tight, semi-tight, and completely loose. The dynamic responses of the system are saved. After obtaining the dynamic responses for these states, the Haar filter bank is used for signal decomposition, followed by using the Smoothed Pseudo Wigner–Ville distribution to reveal the loosening of the bolted flange. It should also be noted that to create an appropriate digital twin, the results of the computer model for the states must, like the experimental results, include the loosening characteristic to ensure the proper training and testing of the convolutional neural network. Therefore, by applying the methods to process the computer-model dynamic responses, this approach is also applied to experimental model data with faulty states. Using the Smoothed Pseudo Wigner–Ville images obtained from the computer model, convolutional neural networks are trained with only healthy experimental model images, and ultimately, the network will be tested using faulty experimental data and images.

Existing vibration-based diagnostic studies often separate numerical modeling from data-driven fault identification, which can compromise either physical interpretability or adaptability to unseen conditions. To address this limitation, the present work develops a digital twin-oriented framework in which numerical simulations and learning-based inference are tightly coupled. The framework employs Haar filter bank decomposition to preprocess vibration signals, followed by time–frequency characterization using the Smoothed Pseudo Wigner–Ville distribution, while fault states are identified through a convolutional neural network. Unlike purely data-driven schemes, the numerical model actively informs the learning stage, enabling reliable diagnosis under limited faulty data conditions. This coupling is particularly suited for monitoring bolted flange systems, where partial loosening and contact nonlinearity play a critical role. Figure 1 presents the flowchart of the proposed method for Haar filter bank and Smoothed Pseudo Wigner–Ville distribution based on the digital twin approach.

In Section 2, the computer modeling of the flanged pipe using the finite element model will be presented with the necessary explanations. Section 3, titled “Experimental Tests,” consists of two subsections: “Modal Analysis Testing for Model Updating” and “Dynamic Response Extraction Testing for Loosening,” which

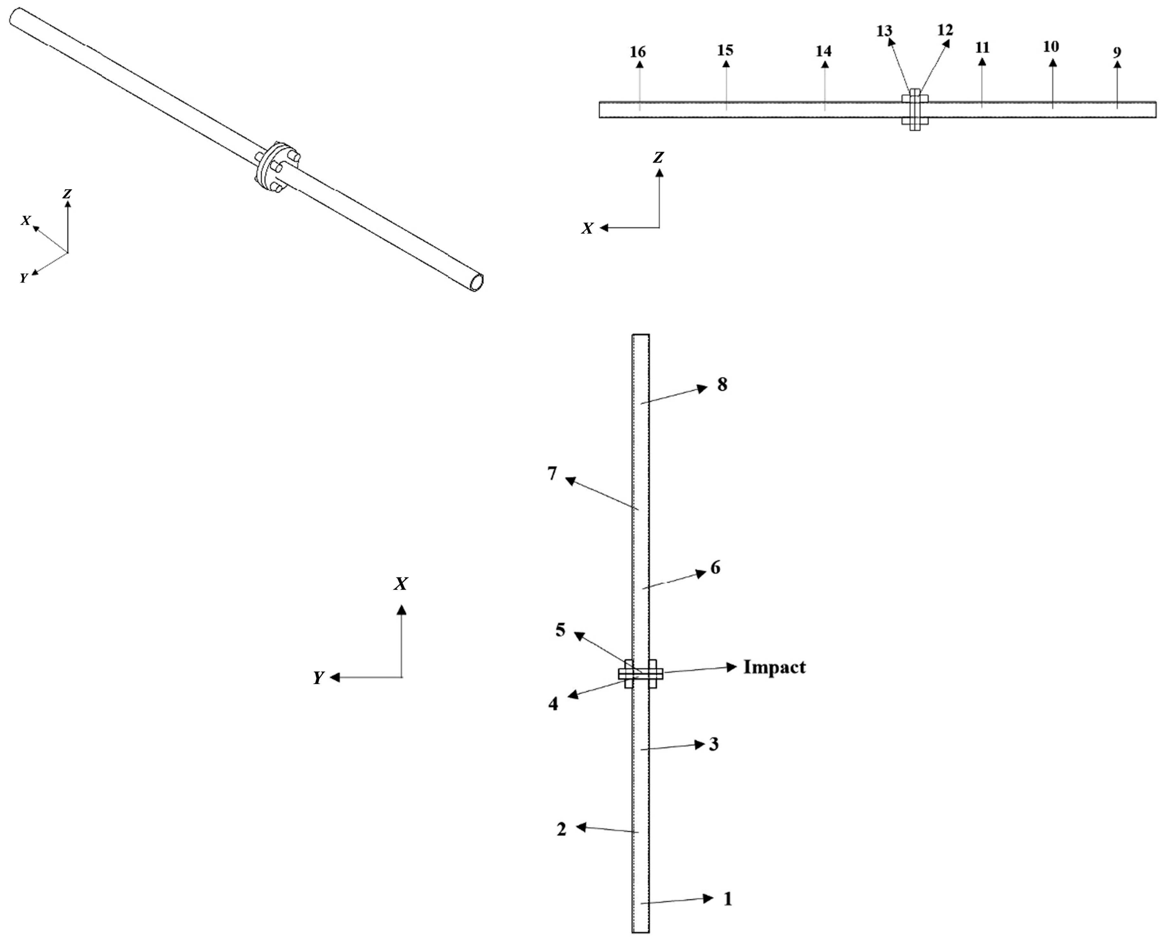

FIGURE 3 | Location of installed sensors and impact points on the flange.

address updating the model parameters and collecting data for the mentioned faulty states, respectively. Section 4 is dedicated to the Haar Filter Bank, Sections 5 and 6 discuss the formulation of Smoothed Pseudo Wigner–Ville distribution and architecture of Convolutional Neural Networks, respectively, and finally, Sections 6 and 7 present the results and conclusion, respectively.

2 | Finite Element Model of the Flanged Pipe

The flanged pipe model shown in Figure 2 is used, and the dimensions are derived from the experimental model. After constructing the model in SolidWorks, it is imported into Abaqus. Given the pipe material, which is steel, Young's modulus (E), density (ρ), and Poisson ratio (ν) are 210 GPa, 7800 kg/m^3, and 0.3, respectively. In the model updating procedure, only Young's modulus and density were selected as updating parameters. This choice is because variations in Young's modulus primarily reflect changes in the structure's global stiffness. At the same time, density directly governs the mass distribution, which in turn has a dominant influence on the system's natural frequencies. In contrast, Poisson ratio has a comparatively minor effect on modal frequencies and was therefore kept constant at its nominal value. Additionally, boundary conditions and bolt preload were defined based on the experimental setup and controlled tightening procedures. They were not treated as updating parameters to avoid parameter coupling and non-uniqueness in the updating process. Limiting the number of updating parameters also improves the robustness, convergence, and physical interpretability of the digital twin calibration. To reduce simulation time, the complexity of surface meshing is minimized, and to avoid defining contacts between them, the bolts and studs are treated as a single body. On the other hand, since a torque wrench is used to fully tighten each bolt in the experimental model at a torque of 50 Nm, the computational model in the mentioned software requires the equivalent tensile force to be applied to the bolts. This is calculated using the generated torque, the coefficient of friction for steel, and the stud diameter, yielding an equivalent tensile force of 12,500 N. Therefore, the bolts are under tension, and the flanges are under pressure. The equivalent pressure on the bolt surface is applied at 32 MPa. It is worth noting that under loosening conditions, the pressure on a single bolt gradually decreases to zero. Additionally, to better simulate the bolts, the friction coefficient between the bolts and flanges is considered, with the appropriate coefficient applied for the different conditions. The boundary conditions for the flanged pipe are set to pin–pin at both ends, so it is not treated as an updating parameter.

FIGURE 4 | Experimental setup.

FIGURE 5 | Measurement equipment: (A) Accelerometer; (B) Impact hammer; (C) Pulse data acquisition system; (D) Torque wrench.

3 | Experimental Tests

To update the model, experimental modal analysis tests are required. The experimental analysis involves exciting the flanged pipe with a hammer and acquiring data with accelerometers, followed by the necessary processing, as explained in Section 3.1. After updating the model, further experimental tests are needed for both the healthy and faulty states, as fully explained in Section 3.2.

3.1 | Modal Analysis Test for Model Updating

After performing the frequency analysis of the finite element model, model parameters need to be updated. In this study, only two parameters, Young's Modulus (E) and Density (ρ), are considered for updating. Initially, four bolts from the real model are tightened to 50 Nm using a torque wrench, and four accelerometers (B&K Co., Type 4507) are installed on the flanged pipe, as shown in Figure 3. A hammer (B&K SV Co., Type 8200) is then used to excite the pipe. The accelerometer sensors are mounted in a roving pattern as shown in Figure 2, and a hammer strike is applied at the indicated locations four times. The data is collected using a data acquisition device (B&K SV Co., Type 22827), and the necessary processing is performed using B&K Co. Pulse software. Figure 4 shows the experimental setup, and Figure 5 displays the equipment used.

3.2 | Experiment for Extracting the Dynamic Response of Bolt Loosening

After validating the finite element model, experimental testing is conducted to obtain the dynamic responses of the fully tightened state under environmental excitations, with the bolts tightened to 50 Nm using a torque wrench. For environmental excitation, a shaker (B&K Co., Type 4809) connected to the flange via a force transducer (PCB Co., Type 27263) is used. The accelerometer locations were selected based on the dominant shapes of the flanged pipe obtained from the finite element model, to maximize sensitivity to vibration changes induced by bolt loosening. White noise signals are applied to excite the flange tube, and an amplifier (B&K Co., Type 2706) is employed to enhance the noise. Figure 6 shows the experimental setup for

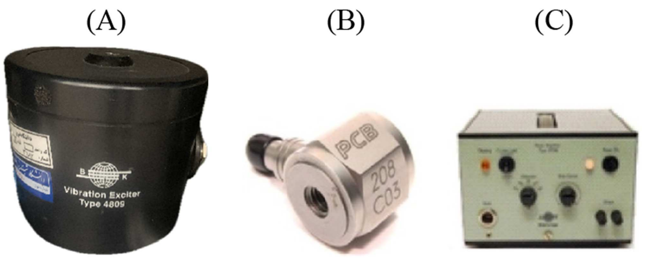

FIGURE 7 | Equipment for conducting the test: (A) Shaker; (B) Force transducer; (C) Amplifier.

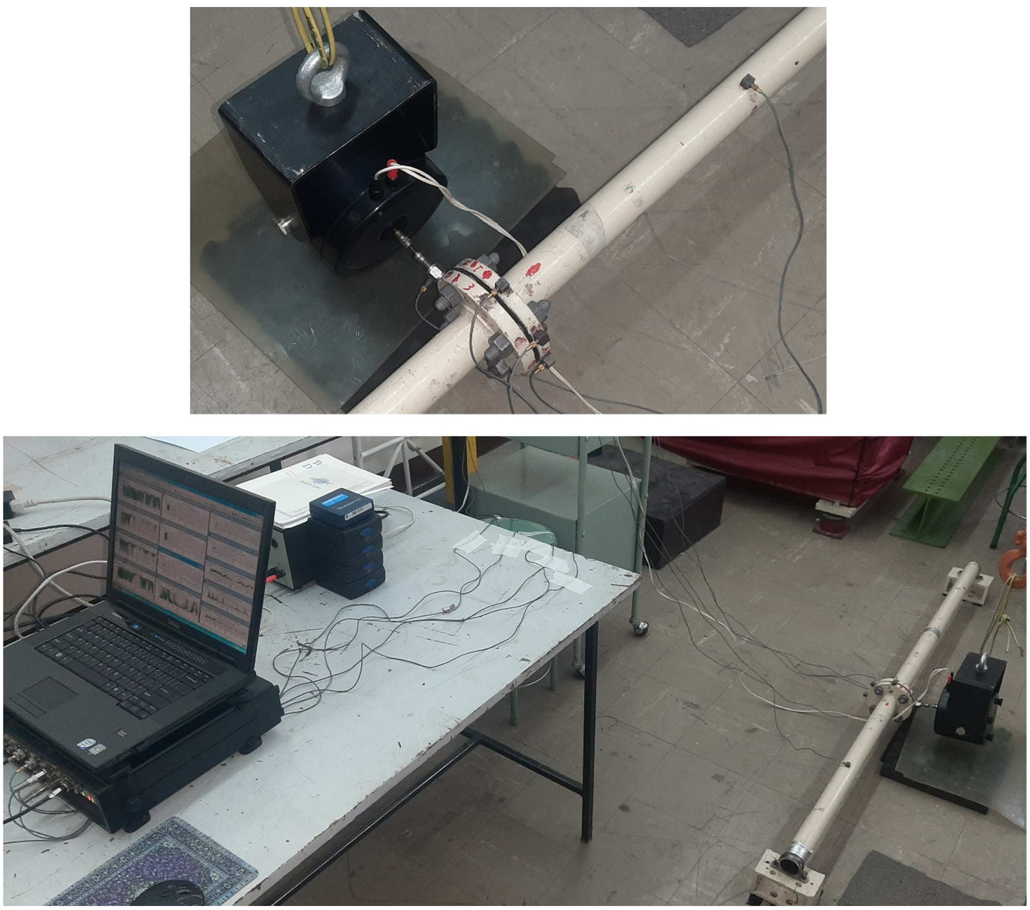

FIGURE 6 | Experimental setup for performing the bolt loosening test.

the bolt loosening dynamic response extraction test, and Figure 7 shows the equipment used. It is noteworthy that, since pipes typically contain various fluids and flow continuously, assuming white noise as the excitation source is a reasonable approximation. In practical operating conditions, piping systems are subjected to broadband and stochastic excitations originating from internal fluid flow, turbulence, pressure fluctuations, and external environmental disturbances. These excitations do not act at a single frequency but instead excite multiple vibration modes simultaneously over a wide frequency range. White noise excitation provides a controlled, repeatable means of replicating these operational conditions in laboratory experiments, ensuring sufficient modal excitation while avoiding bias toward specific frequencies. Consequently, the use of white noise effectively captures and compares the dynamic response characteristics associated with bolt loosening between the experimental setup and the validated finite element model. After the necessary setup, excitation is performed for 2 min for the fully tight state, and data is recorded. Next, a semi-tight state is applied by tightening the bolts to 25 Nm using the torque wrench, and excitation and data recording are performed for this state as well. The selected torque level for the semi-tight condition (25 Nm) corresponds to approximately 50% of the fully tightened state, which is commonly adopted in experimental studies to represent partial loosening in bolted joints. Finally, for the fully loose state of one bolt, the same procedure is repeated, and the time-series signals for the different states are stored. It is also worth noting that the finite element model is simulated for 1 min for each state using a white-noise excitation signal. Time-series signals are recorded from the nodes corresponding to the accelerometer locations in the real experiment. Figure 8 shows the red bolt, which is the target for fault diagnosis. After validating the finite element model through experimental modal analysis and ensuring consistency between the numerical and experimental dynamic responses, the developed model is treated as a physics-informed digital twin of the flanged pipe system. At this stage, both numerical and experimental vibration responses provide a reliable basis for extracting fault-sensitive features associated with bolt loosening. However, the raw time-domain signals contain multiple frequency components and transient characteristics that are not directly suitable for pattern recognition. Therefore, advanced signal decomposition and time–frequency analysis techniques are required to transform the validated digital twin responses into discriminative representations that can be effectively used for convolutional neural network-based fault classification.

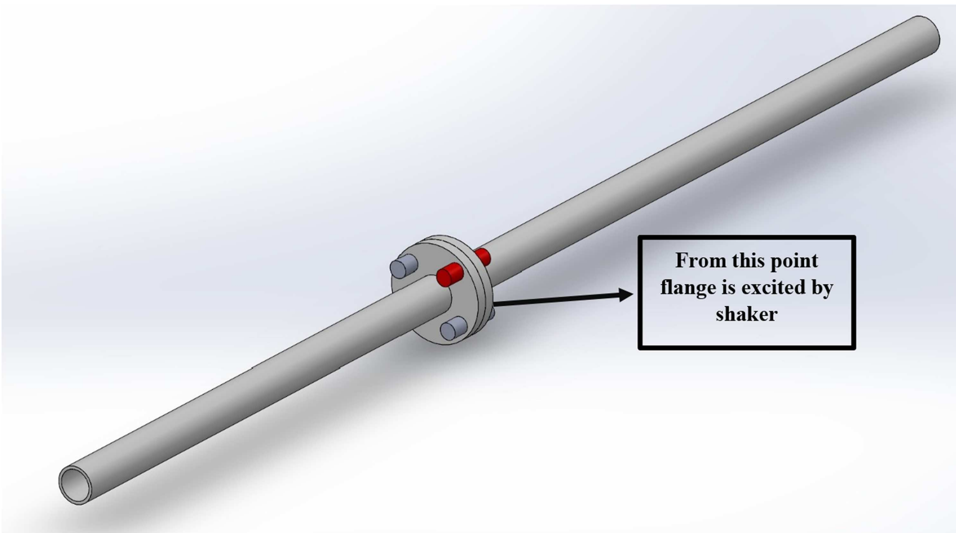

FIGURE 8 | The red bolt indicates the bolt of interest for fault diagnosis.

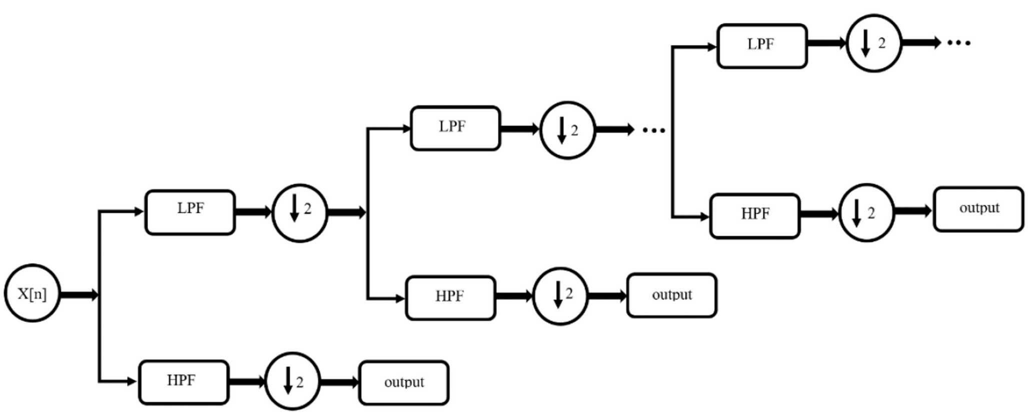

FIGURE 9 | Multilevel decomposition scheme of the Haar filter bank.

4 | Haar Filter Bank

The measured dynamic response of the structure exhibits a multi-frequency nature, where distinct spectral components reflect different aspects of the system behavior. Direct utilization of the raw signal is therefore insufficient for reliable fault-related feature identification, making a preliminary signal decomposition stage essential. A Haar filter-bank framework is adopted here to hierarchically separate the response into complementary low and high-frequency sub-bands, as formulated in Equations (1) and (2). This decomposition is applied recursively to the low-frequency branch, enabling latent defect-sensitive information to be progressively transferred into higher-frequency components, which are subsequently exploited for feature extraction and diagnostic analysis. The structure of the Haar filter bank is shown in Figure 9. It should be noted that, in this study, the Haar filter bank is employed as a multiresolution signal decomposition tool rather than a classical discrete or continuous wavelet transformation. Although the Haar filter bank is mathematically related to the Haar wavelet, the focus here is on its filter-based implementation for frequency band separation and feature enhancement, rather than on wavelet coefficient analysis.

$$\mathrm{LPF} = \frac{X[n] + X[n-1]}{2} \tag{1}$$

$$\mathrm{HPF} = \frac{X[n] - X[n-1]}{2} \tag{2}$$

In the above formulation, $x[n]$ denotes the input signal applied to the filter bank, while $x[n-1]$ corresponds to its one-sample shifted version. Following the filtering stage, the resulting sub-band signals are downsampled by a factor of two to preserve critical frequency content. The decomposition is then continued in a cascaded manner by feeding the low-frequency output back into the filter bank at subsequent levels. At each stage, the high-frequency branch is retained as the primary output for further analysis, whereas the low-frequency branch serves as the input for the next decomposition level. This iterative process is repeated until the signal components exhibit sufficient resolution and sensitivity for reliable feature extraction. One stage of decomposition is selected, and after that, the SPWVD is applied to both the model and experimental signals. One minute of the experimental signal is stored in the time domain using a 1-s sliding window, without overlapping, as shown in Figure 10. Each 1-s signal is then decomposed into six components using the proposed filter bank, and the Smooth Pseudo-Wigner distribution is applied to each component, yielding a total of 30 sets of signals. It should be noted that

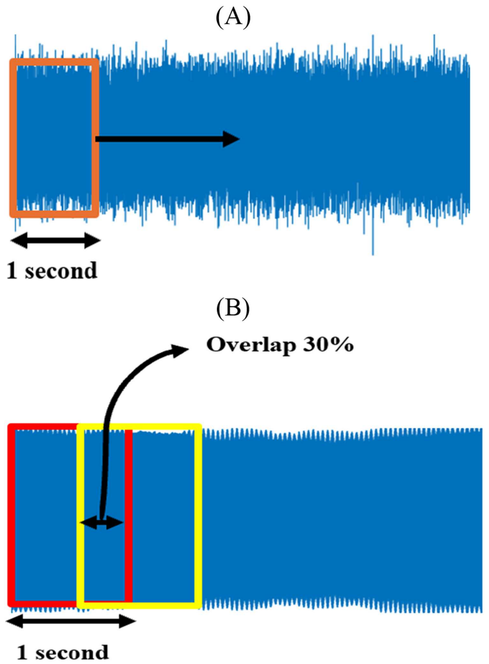

FIGURE 10 | Sliding time window: (A) Experimental signal; (B) Finite element signal.

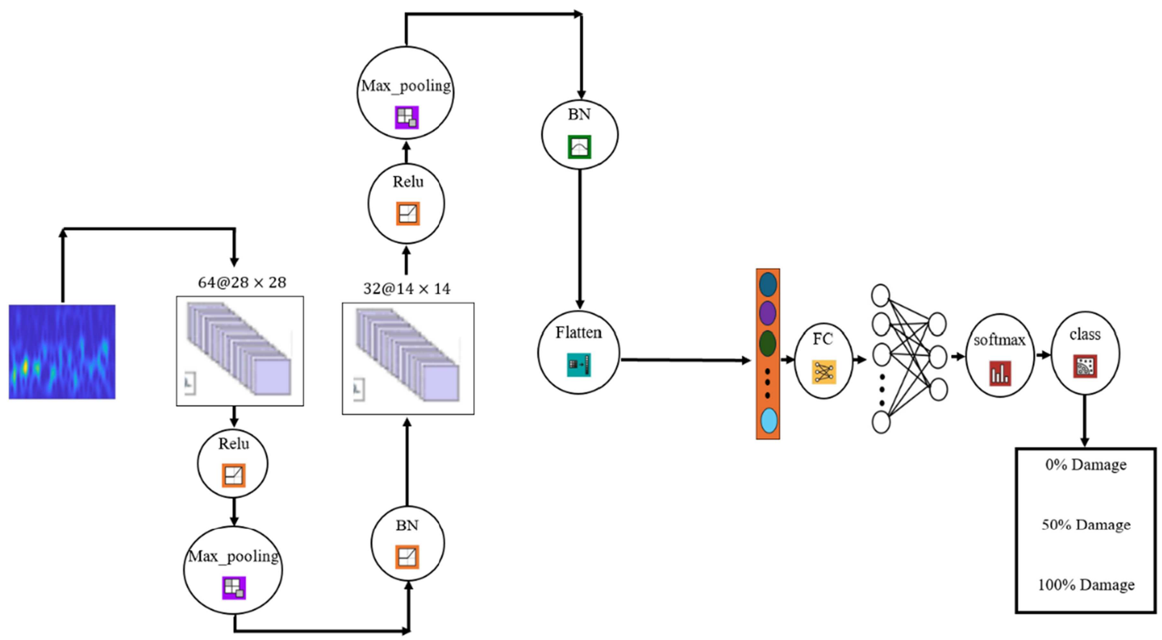

FIGURE 11 | Proposed architecture of convolutional neural networks.

different decomposition levels are adopted for the experimental and numerical signals due to differences in sampling frequency and computational constraints. The experimental signals are acquired with a higher sampling frequency, allowing a six-level Haar decomposition to achieve finer frequency resolution for feature extraction. In contrast, to perform long-duration simulations under white noise excitation while maintaining reasonable computational cost, the finite element model is simulated with a sampling frequency of 2000 Hz, which is lower than that of the experimental measurements. Therefore, a four-level decomposition is selected for the numerical model to ensure that the resulting frequency bands are comparable to those obtained from the experimental data. This approach guarantees consistency in the effective frequency range analyzed across both models, while enabling deeper decomposition of the experimental signals for improved fault-feature discrimination. Due to the system computational-modeling limitations, a 1-min simulation is performed at a sampling frequency of 2000 Hz, with a 1 s sliding window with 30% overlap, as shown in Figure 10. It is worth mentioning that for consistency in the frequency range between the computational model and the experimental model, decomposition is performed in four stages, and for each state, 85 time-series signals are obtained for 1 min (1×2000), resulting in a total of (85×2000) data.

5 | Smoothed Pseudo Wigner–Ville Distribution

The Wigner–Ville distribution provides a mapping of non-stationary signals into the time–frequency domain,

TABLE 2 | Natural frequencies (Hz) before and after the update of the finite element model and experimental modal analysis.

	Finite element model	
Experimental modal analysis frequencies	**Before update**	**After update**
61.8	76.213	62.791
214	261.81	216.38
374	488.9	404.07
615	794.68	656.8
981	1196.3	998.7

TABLE 1 | Full architectural and configuration description of the proposed network.

Type of layer	Number of convolution kernels	Size of kernel	Activation function	Stride
Convolution 2-D	64	28 × 28	Relu	14
Max_Pooling 2-D	64	2 × 2	—	2
Convolution 2-D	32	14 × 14	Relu	7
Max_Pooling 2-D	32	2 × 2	—	2
Flatten	—	—	—	—
Fully connected	—	—	SoftMax	—
Classify	—	—	—	—

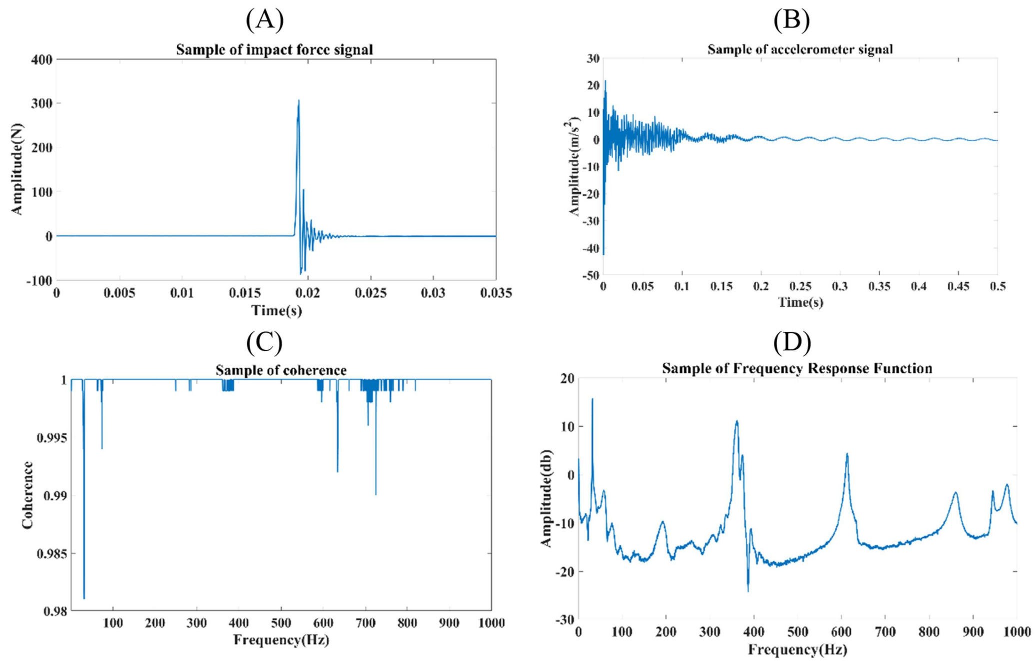

FIGURE 12 | A sample of the results of the updating model: (A) Sample of impact force signal; (B) Sample of accelerometer signal; (C) Sample of coherence; (D) Sample of frequency response function.

allowing the instantaneous distribution of signal energy to be examined with high resolution. Unlike the short-time Fourier transform, whose resolution is constrained by a fixed analysis window, this representation captures rapid energy variations without imposing a time–frequency trade-off. From a theoretical perspective, the Wigner–Ville distribution belongs to the class of bilinear time–frequency representations. It is obtained by applying a Fourier transform with respect to the lag variable to the instantaneous autocorrelation function of the signal. For a non-stationary random process, the resulting formulation is defined by the following equation:

$$\mathrm{WVD}(t, f) = \int_{-\infty}^{\infty} x\left(t + \frac{\tau}{2}\right) x^*\left(t - \frac{\tau}{2}\right) \mathrm{e}^{-\mathrm{j}2\pi f\tau}\, \mathrm{d}\tau \tag{3}$$

Equation (3) represents the Wigner–Ville distribution, where the operator $(\cdot)^*$ indicates complex conjugation. The formulation relies on a time-shifted autocorrelation of the signal, whose spectral content is obtained through a Fourier transform with respect to the lag parameter.

$$x\left(t\right)_a = x\left(t\right) + jx\left(t\right)_h \tag{4}$$

For time–frequency analysis, the signal $\boldsymbol{x}(\boldsymbol{t})$ is expressed in its analytic form, as given in Equation (4), in which the imaginary component is defined by the Hilbert transform of the original signal. The Hilbert transform, which ensures suppression of negative-frequency components and facilitates a physically meaningful energy representation, is defined by the following equation:

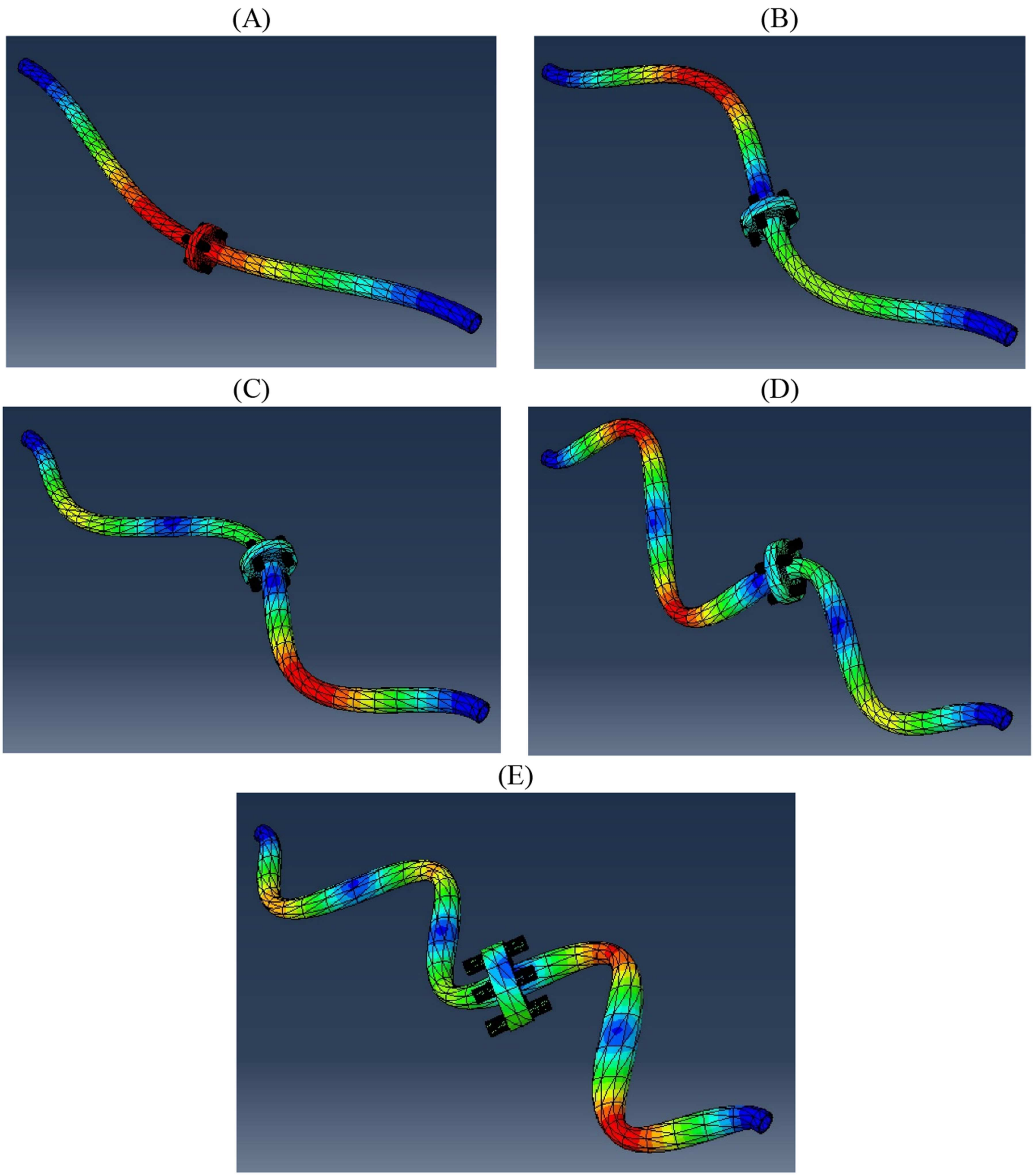

FIGURE 13 | Mode shapes correspond to the natural frequencies: (A) First mode; (B) Second mode; (C) Third mode; (D) Fourth mode; (E) Fifth mode.

$$H(x(t)) = x(t)_h = \frac{1}{\pi}\int_{-\infty}^{\infty} x(\tau)\frac{1}{t-\tau}\mathrm{d}\tau \tag{5}$$

Introducing a temporal window function into the lag domain leads to the PWVD. This windowing operation reduces interference terms while preserving the principal time–frequency structure of the signal. The PWVD is defined as

$$\mathrm{PWVD}\left(t, f\right) = \int_{-\infty}^{\infty} x\left(t + \frac{\tau}{2}\right)x^*\left(t - \frac{\tau}{2}\right)h\left(\tau\right)\mathrm{e}^{-\mathrm{j}2\pi f\tau}\,\mathrm{d}\tau \tag{6}$$

Further smoothing is achieved by incorporating an additional kernel function, resulting in the smoothed pseudo-Wigner–Ville distribution expressed in Equation (7) below. The combined application of windowing and smoothing functions enhances the readability of the time–frequency representation and improves its suitability for subsequent feature extraction and learning-based analysis.

$$\mathrm{SPWVD}(t, f) = \int_{-\infty}^{\infty} h(\tau)\int_{-\infty}^{\infty} g(u-\tau)x\left(t+\frac{\tau}{2}\right)x^*\left(t-\frac{\tau}{2}\right)h(\tau)\mathrm{e}^{-\mathrm{j}2\pi f\tau}\,\mathrm{d}\tau \tag{7}$$

6 | Convolutional Neural Networks

When using the Smoothed Pseudo-Wigner–Ville distribution for the filter-bank output signals, the results are in image form. Using neural networks to classify the extracted images poses complex challenges. In recent studies, convolutional neural networks (CNNs) have been proposed for classification. The main goal in designing the network is to have the simplest architecture with the most accurate response. The fewer the network hidden layers, while maintaining high efficiency, the shorter the learning time will be. The network architecture is shown in Figure 11. In each convolutional layer, the image is convolved with a matrix, or kernel. The Leaky ReLU activation function is then used to activate the output. Max pooling produces a matrix of specified dimensions by selecting and storing the maximum value at each location. Batch normalization speeds up network training by reducing the need for complex calculations by normalizing the matrices. The Leaky ReLU activation function is selected to address potential vanishing gradients and neuron inactivation issues that may arise when processing sparse, high-contrast time–frequency images generated by the Smoothed Pseudo Wigner–Ville distribution. Unlike the standard ReLU function, Leaky ReLU allows a small gradient for negative inputs, improving training stability and ensuring that informative low-energy features related to early-stage bolt loosening are not discarded. Max pooling layers are employed to reduce the spatial dimensionality of the feature maps while preserving the most salient fault-related features. This operation increases robustness against local noise and minor signal variations, improves generalization, and reduces computational complexity, which is consistent with maintaining a simple yet effective network architecture. Flattening converts multi-dimensional matrices into column vectors, which, with fully connected layers, update the network weights at each iteration.

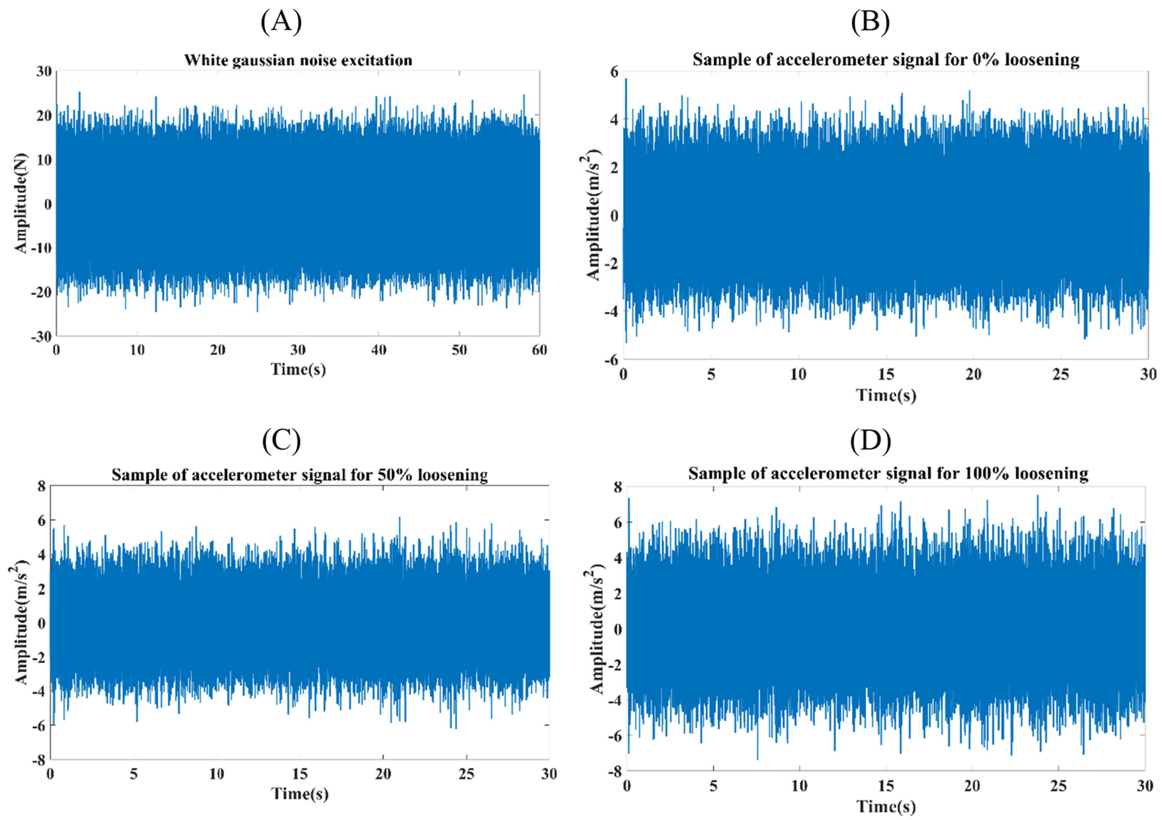

FIGURE 14 | A sample of the signals for the faulty state: (A) For force transducer; (B) For 0% loosening; (C) For 50% loosening; (D) For 100% loosening.

Finally, the network classifies the defect classes using SoftMax. The extracted images for each state, using the 1-s segmentation and the mentioned window for the computational model responses, are 85 in total. For network training, in addition to the images from the model, images from the healthy state of the experimental model are also used. In the end, 115 images for the healthy state and 170 images for the defective states are used for network training and validation. A total of 30 images per state from the experimental model are extracted and used to test the network. The structural specifications and key parameters of the neural networks are reported in Table 1.

7 | Results and Discussion

7.1 | Results of the Model Updating

As mentioned, to update the model initially, an experimental modal analysis test was conducted: the pipe flange was excited with a hammer, and data were collected with an accelerometer. Furthermore, the accuracy of the experimental modal analysis test, which is affected by noise levels, is particularly important. For this purpose, the level of noise in the frequency response function is determined from the coherence plot. Additionally, the accuracy of the output-to-input ratio is measured using this criterion. The closer the value is to one, the more it indicates that the output-to-input transfer has been carried out with high accuracy. Finally, the obtained frequency response functions for the completely tight condition are used to extract the system natural frequencies for model updating, which are determined using the Mescope software and curve-fitting methods. The finite element model updating was performed through an iterative calibration procedure to improve the agreement between experimentally identified and numerically predicted natural frequencies. In each iteration, Young's modulus and material density of the finite element model were adjusted, and the resulting natural frequencies were compared with those obtained from the experimental modal analysis. The updating process was continued until the discrepancies between the

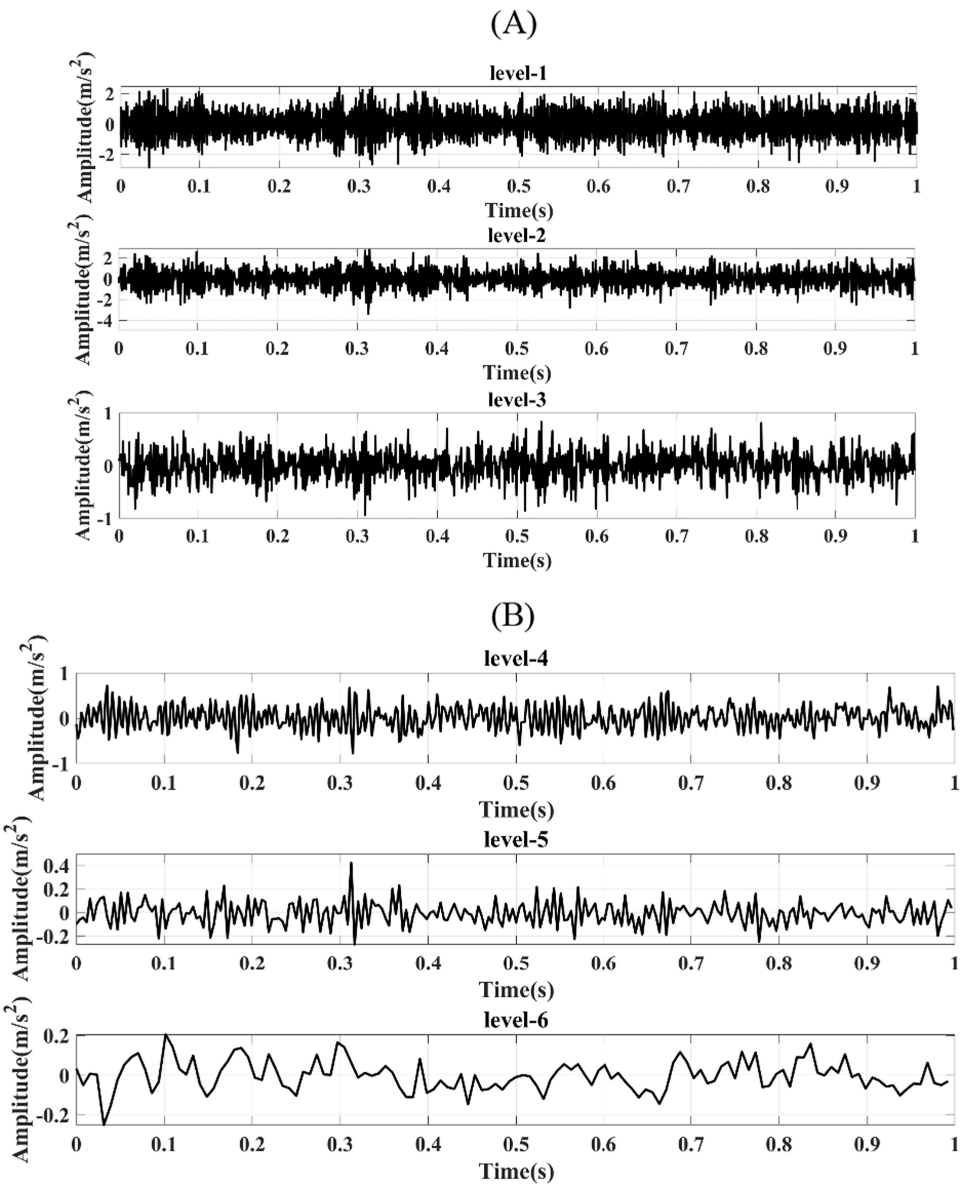

FIGURE 15 | Decomposed signal of one of the 1-s segments for the completely healthy state: (A) The first three levelsof decomposition; (B) The second three levels of decomposition.

experimental and numerical natural frequencies were reduced to an acceptable level, and further parameter adjustments yielded negligible improvement. This ensured that the calibrated finite element model accurately represents the dynamic behavior of the physical structure. Figure 12 shows an example of the impact signal, accelerometer signal, coherence, and frequency response function. The natural frequencies before and after updating are shown in Table 2, and the corresponding mode shapes are shown in Figure 13. The remaining discrepancies between the updated finite element model and the experimental natural frequencies can be attributed to modeling simplifications, such as idealized boundary conditions and an approximate representation of bolted joint contact behavior. Effects including friction, micro-slips, and preload-dependent nonlinear stiffness were not explicitly modeled. However, these discrepancies mainly influence the absolute frequency values, while the relative dynamic response variations caused by bolt loosening remain sufficiently captured for reliable fault detection.

7.2 | Results of the Proposed Fault Detection Method Test

After completing the model updating stages, the bolt-loosening experiment is conducted, using a torque wrench to apply torque at the semi-loosened and fully loosened conditions. In each of these states, the shaker exciting the flanged pipe with a white noise signal, and data is collected using accelerometers. Figure 14 shows a sample of the force sensor and accelerometer signals for the states mentioned.

After recording the signals for each of the states mentioned, the signals are separated into 1-s segments, and the Haar filter bank is applied to each state, decomposing the signal to six levels. Figure 15 shows the decomposed signal of one of the 1-s segments for the completely tight state.

Following signal decomposition, the Smoothed Pseudo Wigner–Ville distribution is computed for each condition using the sixth-level components. The same processing workflow is consistently applied to the responses obtained from the numerical model. Owing to differences in sampling frequency, the simulated signals are decomposed into a maximum of four levels, after which the SPWVD is evaluated. Figure 16 shows the energy of each state for comparison.

As shown in Figure 16, energy changes with the severity of the defect, which holds true for both the experimental and computational models. To classify the obtained images, convolutional neural networks have been proposed, trained with the Adam solver and then validated. The learning rate is set to 0.001, and the maximum epoch is 50. During training and

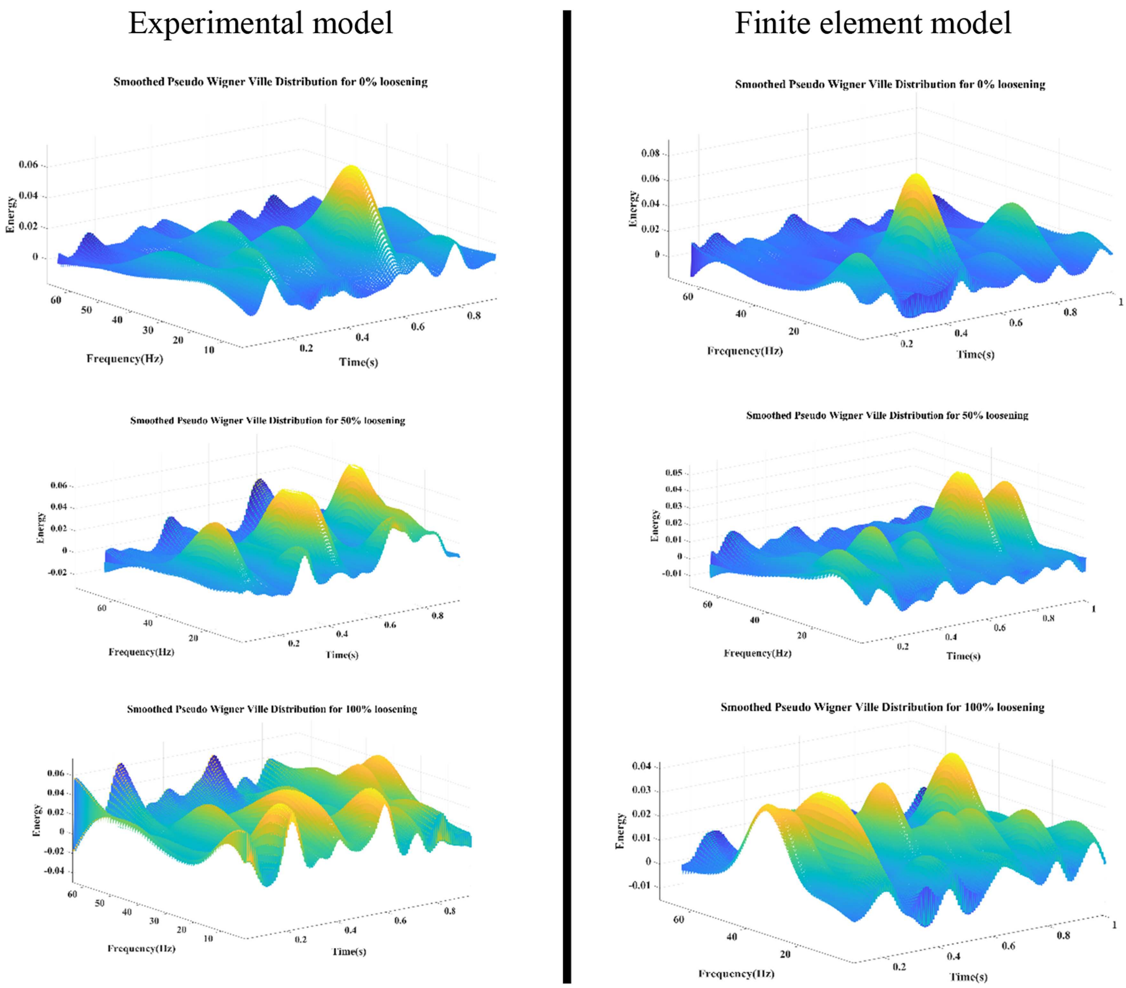

FIGURE 16 | SPWVD results for simulated and experimental responses.

validation, the neural networks are shown in Figure 17 across the iterations.

As illustrated in Figure 17, the proposed neural networks exhibit stable convergence during training and achieve classification accuracies exceeding 90%. To verify that the learned representations generalize beyond the training samples, an independent validation phase is conducted, yielding comparable accuracy levels. The learning behavior of the networks is further evidenced by the trend of the loss functions, where a consistent decrease in both training and validation losses reflects stable convergence. A noticeable separation between these curves would imply overfitting; however, their closely aligned evolution demonstrates that the models have learned transferable and well-generalized decision mechanisms rather than memorizing the training samples. Although the convolutional neural network is trained solely on healthy experimental data and numerical model data, potential overfitting is carefully addressed. A compact network architecture with a limited number of convolutional layers is intentionally adopted to reduce model complexity. Batch normalization is employed to stabilize the learning process and improve generalization. In addition, validation is performed during training to monitor the divergence between training and validation loss. As illustrated in Figure 17, the convergence of both accuracy and loss curves demonstrates stable learning behavior without overfitting. Finally, the trained network is tested exclusively using unseen faulty experimental data, and the resulting confusion matrix in Figure 18 confirms the robustness and generalization capability of the proposed approach.

As shown in the confusion matrix (Figure 18), most misclassifications occur in the semi-tight condition, which represents a transitional state between fully tight and fully loose configurations. The overlap in dynamic response characteristics for this intermediate condition increases classification difficulty. Nevertheless, the proposed network achieves high overall accuracy, indicating that the extracted time–frequency features remain sufficiently discriminative for reliable fault diagnosis.

8 | Conclusion

Fault detection in bolted connections is of particular importance to researchers and engineers, as their complex nature poses significant challenges. On the other hand, computer modeling of connections has always attracted the attention of engineers and researchers under various theories. Today, with the use of computer modeling and the proposal of appropriate feature-extraction methods for extracting fault-sensitive parameters, a

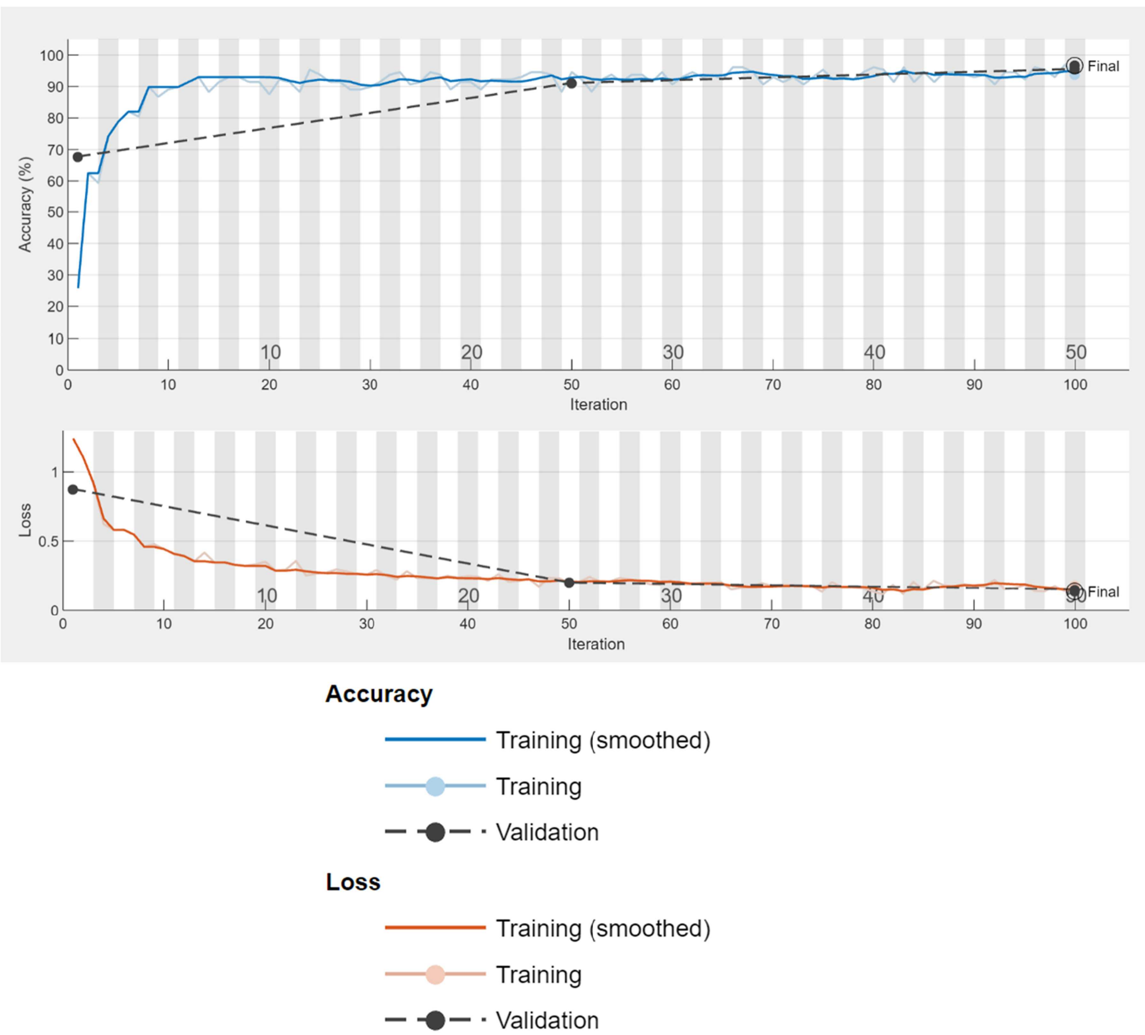

FIGURE 17 | Training procedure of the neural network.

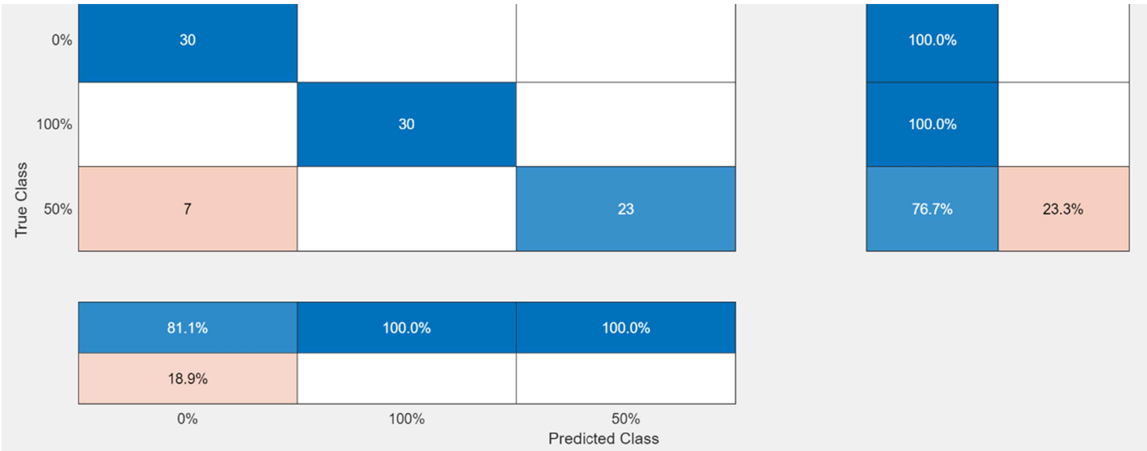

FIGURE 18 | Confusion matrix.

new method known as the digital twin has been introduced. In this study, computer modeling of a pipe flange with bolted connections was first performed. After extracting the system natural frequencies, the model parameters were updated. For this purpose, an experimental modal analysis was conducted on the experimental model to determine the system natural frequencies, which served as a reference for updating the model parameters. In this study, only Young's modulus and the overall density of the system were considered as the two parameters for model updating and updating them resulted in the computational model natural frequencies becoming closer to those of the experimental model. After updating the computational model, it was found to be faulted, with the bolted connection loosened to a semi-loose and fully loose state. For each of these conditions, the system dynamic response was recorded. After saving dynamic responses and simulations, Haar filter bank was applied, and the signals were decomposed. Then, the output of a specific decomposition level was used to apply the Smoothed Pseudo-Wigner–Ville distribution. Data from the computational model, along with data from only the healthy experimental model, were used to train the network. For testing the trained networks, dynamic response data from the faulty states of the experimental model was used. Finally, the method resulting from the proposed test achieved over 90%, indicating its success.

Acknowledgments

Open access publishing facilitated by James Cook University, as part of the Wiley—James Cook University agreement via the Council of Australasian University Librarians.

Funding

The authors have nothing to report.

Conflicts of Interest

The authors declare no conflicts of interest.

Data Availability Statement

The data that support the findings of this study are available on request from the corresponding author. The data is not publicly available due to privacy or ethical restrictions.

References

1. P. Thananjayan, S. Natarajan, and P. Ramu, "Image-Based Flaw Identification Using Convolutional Neural Network," *International Journal of Mechanical System Dynamics* 5, no. 4 (2025): 694–706.

2. G. Dessena, M. Civera, A. Yousefi, and C. Surace, "NExT-LF: A Novel Operational Modal Analysis Method via Tangential Interpolation," *International Journal of Mechanical System Dynamics* 5, no. 3 (2025): 401–414.

3. I. Khalid, Z. A. Qureshi, F. Siddiqui, S. Oterkus, and E. Oterkus, "Structural Health Monitoring of Thin Shell Structures," *International Journal of Mechanical System Dynamics* 5, no. 1 (2025): 20–39.

4. K. He and W. Zhu, "Finite Element Modeling of Structures With L-Shaped Beams and Bolted Joints," *Journal of Vibration and Acoustics* 133 (2011): 011011.

5. S. Bograd, P. Reuss, A. Schmidt, L. Gaul, and M. Mayer, "Modeling the Dynamics of Mechanical Joints," *Mechanical systems and signal processing* 25, no. 8 (2011): 2801–2826.

6. H. Zerres and Y. Guérout, "Present Calculation Methods Dedicated to Bolted Flanged Connections," *International Journal of Pressure Vessels and Piping* 81, no. 2 (2004): 211–216.

7. W. C. Xing, J. Wang, and Y. Q. Wang, "An Effective Model for Bolted Flange Joints and Its Application in Vibrations of Bolted Flange Joint Multiple-Plate Structures: Theory With Experiment Verification," *Applied Mathematical Modelling* 126 (2024): 482–505.

8. Y. Zhao, Y. Zhang, J. Wang, Q. Yue, and H. Chen, "Comparison of Non-Destructive Testing Methods of Bolted Joint Status in Steel Structures," *Measurement* 242 (2024): 116318.

9. L. Zheng, L. Wang, L. Zhu, et al., "Analytical Model of the Shear Behaviors of Bolted Rough Joints Based on the Dilation Effect and Surface Abrasion," *Engineering Geology* 294 (2021): 106399.

10. H. Ouyang, M. J. Oldfield, and J. E. Mottershead, "Experimental and Theoretical Studies of a Bolted Joint Excited by a Torsional Dynamic Load," *International Journal of Mechanical Sciences* 48, no. 12 (2006): 1447–1455.

11. Q. Tang, C. Li, H. She, and B. Wen, "Vibration Analysis of Bolted Joined Cylindrical-Cylindrical Shell Structure Under General Connection Condition," *Applied Acoustics* 140 (2018): 236–247.

12. T. Yang, H. Ma, Z. Qin, H. Guan, and Q. Xiong, "Coupling Vibration Characteristics of the Shaft-Disk-Drum Rotor System With Bolted Joints," *Mechanical Systems and Signal Processing* 169 (2022): 108747.

13. N. Jamia, H. Jalali, J. Taghipour, M. I. Friswell, and H. Haddad Khodaparast, "An Equivalent Model of a Nonlinear Bolted Flange Joint," *Mechanical Systems and Signal Processing* 153 (2021): 107507.

14. H. Jalali, H. Ahmadian, and J. E. Mottershead, "Identification of Nonlinear Bolted Lap-Joint Parameters by Force-State Mapping," *International Journal of Solids and Structures* 44, no. 25–26 (2007): 8087–8105.

15. R. Lacayo, L. Pesaresi, J. Groß, et al., "Nonlinear Modeling of Structures With Bolted Joints: A Comparison of Two Approaches Based on a Time-Domain and Frequency-Domain Solver," *Mechanical Systems and Signal Processing* 114 (2019): 413–438.

16. C. W. Schwingshackl, D. Di Maio, I. Sever, and J. S. Green, "Modeling and Validation of the Nonlinear Dynamic Behavior of Bolted Flange Joints," *Journal of Engineering for Gas Turbines and Power* 135, no. 12 (2013): 122504.

17. L. Gaul and J. Lenz, "Nonlinear Dynamics of Structures Assembled by Bolted Joints," *Acta Mechanica* 125, no. 1 (1997): 169–181.

18. S. I. Zare Estakhraji, M. Wall, J. Capito, and M. S. Allen, "A Thorough Comparison Between Measurements and Predictions of the Amplitude Dependent Natural Frequencies and Damping of a Bolted Structure," *Journal of Sound and Vibration* 544 (2023): 117397.

19. X. Liu, W. Sun, H. Liu, D. Du, and H. Ma, "Nonlinear Vibration Modeling and Analysis of Bolted Thin Plate Based on Non-Uniformly Distributed Complex Spring Elements," *Journal of Sound and Vibration* 527 (2022): 116883.

20. L. Tan, C. Wang, Y. Liu, W. Sun, and W. Zhang, "Study on Hysteresis and Threaded Fitting Behavior of Bolted Joint With Non-Parallel Bearing Surface," *Mechanical Systems and Signal Processing* 168 (2022): 108655.

21. R. A. Ibrahim and C. L. Pettit, "Uncertainties and Dynamic Problems of Bolted Joints and Other Fasteners," *Journal of Sound and Vibration* 279, no. 3–5 (2005): 857–936.

22. I. Argatov and I. Sevostianov, "Health Monitoring of Bolted Joints via Electrical Conductivity Measurements," *International Journal of Engineering Science* 48, no. 10 (2010): 874–887.

23. J. M. Nichols, S. T. Trickey, M. Seaver, S. R. Motley, and E. D. Eisner, "Using Ambient Vibrations to Detect Loosening of a Composite-to-Metal Bolted Joint in the Presence of Strong Temperature Fluctuations," *Journal of Vibration and Acoustics* 129 (2007): 710–717.

24. S. Ritdumrongkul and Y. Fujino, "Identification of the Location and Level of Damage in Multiple-Bolted-Joint Structures by PZT Actuator-Sensors," *Journal of Structural Engineering* 132, no. 2 (2006): 304–311.

25. Y. Luan, Z. Q. Guan, G. D. Cheng, and S. Liu, "A Simplified Nonlinear Dynamic Model for the Analysis of Pipe Structures With Bolted Flange Joints," *Journal of Sound and Vibration* 331, no. 2 (2012): 325–344.

26. W. Shi and Z. Zhang, "Nonlinear Vibration Mechanism and Modeling for Flange-Bolted Joints," *Mechanical Systems and Signal Processing* 211 (2024): 111183.

27. Z. Wu, S. A. Nassar, and X. Yang, "Nonlinear Deformation Behavior of Bolted Flanges Under Tensile, Torsional, and Bending Loads," *Journal of Pressure Vessel Technology* 136, no. 6 (2014): 061201.

28. H. Li, Z. Zou, Y. Yan, et al., "Free and Forced Vibrations of Composite Cylindrical–Cylindrical Shells With Partial Bolt Loosening Connections: Theoretical and Experimental Investigation," *Thin-Walled Structures* 179 (2022): 109671.

29. M. Murali Krishna, M. S. Shunmugam, and N. Siva Prasad, "A Study on the Sealing Performance of Bolted Flange Joints With Gaskets Using Finite Element Analysis," *International Journal of Pressure Vessels and Piping* 84, no. 6 (2007): 349–357.

30. W. H. Semke, G. D. Bibel, S. Jerath, S. B. Gurav, and A. L. Webster, "Efficient Dynamic Structural Response Modelling of Bolted Flange Piping Systems," *International Journal of Pressure Vessels and Piping* 83, no. 10 (2006): 767–776.

31. B. T. Bonab, M. H. Sadeghi, and M. M. Ettefagh, "Bolt Looseness Detection in Flanged Pipes Using Parametric Modeling," *Journal of Pipeline Systems Engineering and Practice* 16, no. 1 (2025): 04024067.

32. K. He and W. D. Zhu, "Detecting Loosening of Bolted Connections in a Pipeline Using Changes in Natural Frequencies," *Journal of Vibration and Acoustics* 136, no. 3 (2014): 034503.

33. P. Razi, R. A. Esmaeel, and F. Taheri, "Improvement of a Vibration-Based Damage Detection Approach for Health Monitoring of Bolted Flange Joints in Pipelines," *Structural Health Monitoring* 12, no. 3 (2013): 207–224.

34. Y.-J. Cha, R. Ali, J. Lewis, and O. Büyüköztürk, "Deep Learning-Based Structural Health Monitoring," *Automation in Construction* 161 (2024): 105328.

35. Z. Mousavi, S. Varahram, M. M. Ettefagh, M. H. Sadeghi, W. Q. Feng, and M. Bayat, "A Digital Twin-Based Framework for Damage Detection of a Floating Wind Turbine Structure Under Various Loading Conditions Based on Deep Learning Approach," *Ocean Engineering* 292 (2024): 116563.

36. Z. Mousavi, S. Varahram, M. Mohammad Ettefagh, and M. H. Sadeghi, "Dictionary Learning-Based Damage Detection Under Varying Environmental Conditions Using Only Vibration Responses of Numerical Model and Real Intact State: Verification on an Experimental Offshore Jacket Model," *Mechanical Systems and Signal Processing* 182 (2023): 109567.

37. Z. Mousavi, S. Varahram, M. M. Ettefagh, M. H. Sadeghi, and S. N. Razavi, "Deep Neural Networks-Based Damage Detection Using Vibration Signals of Finite Element Model and Real Intact State: an Evaluation via a Lab-Scale Offshore Jacket Structure," *Structural Health Monitoring* 20, no. 1 (2021): 379–405.

38. Z. Huang, X. Yin, Y. Liu, and Y. Liu, "Damage Identification of Truss Bridges Based on Feature Transferable Digital Twins," *Measurement* 233 (2024): 114735.

39. M. Fawad, M. Salamak, Q. Chen, et al., "Development of Immersive Bridge Digital Twin Platform to Facilitate Bridge Damage Assessment and Asset Model Updates," *Computers in Industry* 164 (2025): 104189.

40. J. Sánchez-Haro, M. García, G. Capellán, A. Costa, da, P. Perez, and J. Añó, "Digital Twin for Predictive Maintenance on the Espartxo Bridge. Application to Early Detection of Under-Foundation Scour," *Structures* 71 (2025): 107916.

41. D. Chen, C. W. Kim, E. Yoshida, and C. Sim, "Enhancing Structural Damage Evaluation of PC Girder Bridges Through Digital Twinning Bayesian Model Updating," *Engineering Structures* 321 (2024): 118974.

42. G. Shi, Z. Liu, D. Lu, Q. Zhang, Z. Wang, and Y. Zhao, "Digital Twin-Based Model Updating Method for Mechanical Behaviors Analysis of Cable Truss Structure," *Journal of Constructional Steel Research* 221 (2024): 108917.

43. S. C. Jayasinghe, M. Mahmoodian, A. Sidiq, et al., "Innovative Digital Twin With Artificial Neural Networks for Real-Time Monitoring of Structural Response: A Port Structure Case Study," *Ocean Engineering* 312 (2024): 119187.

44. Q. Zhang, S. Zheng, C. Yu, Q. Wang, and Y. Ke, "Digital Thread-Based Modeling of Digital Twin Framework for the Aircraft Assembly System," *Journal of Manufacturing Systems* 65 (2022): 406–420.

45. A. Hasan, T. Asfihani, O. Osen, and R. T. Bye, "Leveraging Digital Twins for Fault Diagnosis in Autonomous Ships," *Ocean Engineering* 292 (2024): 116546.

46. Z. Mousavi, M. M. Ettefagh, M. H. Sadeghi, and S. N. Razavi, "Developing Deep Neural Network for Damage Detection of Beam-Like Structures Using Dynamic Response Based on FE Model and Real Healthy State," *Applied Acoustics* 168 (2020): 107402.

47. Y. Hu, O. W. Taha, and K. Yang, "Fault Detection in Active Magnetic Bearings Using Digital Twin Technology," *Applied Sciences* 14, no. 4 (2024): 1384.

48. S. Gong, S. Li, Y. Zhang, L. Zhou, and M. Xia, "Digital Twin-Assisted Intelligent Fault Diagnosis for Bearings," *Measurement Science and Technology* 35, no. 10 (2024): 106128.

49. T. Wang, K. Feng, J. Ling, et al., "Pipeline Condition Monitoring Towards Digital Twin System: A Case Study," *Journal of Manufacturing Systems* 73 (2024): 256–274.

50. J. Dunyak, X. Gilliam, R. Peterson, and D. Smith, "Coherent Gust Detection by Wavelet Transform," *Journal of Wind Engineering and Industrial Aerodynamics* 77–78 (1998): 467–478.

51. B. H. Kim, T. Park, and G. Z. Voyiadjis, "Damage Estimation on Beam-Like Structures Using the Multi-Resolution Analysis," *International Journal of Solids and Structures* 43, no. 14–15 (2006): 4238–4257.

52. B. H. Kim, H. Kim, and T. Park, "Nondestructive Damage Evaluation of Plates Using the Multi-Resolution Analysis of Two-Dimensional Haar Wavelet," *Journal of Sound and Vibration* 292, no. 1–2 (2006): 82–104.

53. L. Li, L. Qu, and X. Liao, "Haar Wavelet for Machine Fault Diagnosis," *Mechanical Systems and Signal Processing* 21, no. 4 (2007): 1773–1786.

54. K. K. Nair and A. S. Kiremidjian, "Derivation of a Damage Sensitive Feature Using the Haar Wavelet Transform," *Journal of Applied Mechanics* 76 (2009): 061015.

55. K. N. Kesavan and A. S. Kiremidjian, "A Wavelet-Based Damage Diagnosis Algorithm Using Principal Component Analysis," *Structural Control and Health Monitoring* 19, no. 8 (2012): 672–685.

56. K. Jayakumar and S. Thangavel, "A Real Time Data Acquisition and Vibration Analysis Through Wavelet Transform for Fault Detection of Industrial Drives," *Research Journal of Applied Sciences, Engineering and Technology* 9, no. 2 (2015): 122–128.

57. S. Bhattacharya, N. Yadav, A. Ahmad, F. Melandsø, and A. Habib, "Multiple Damage Detection in PZT Sensor Using Dual Point Contact Method," *Sensors* 22, no. 23 (2022): 9161.

58. J. Monieta, "Diagnosing Cracks in the Injector Nozzles of Marine Internal Combustion Engines During Operation Using Vibration Symptoms," *Applied Sciences* 13, no. 17 (2023): 9599.

59. J. Zhang, Z. Zeng, P. K. Sharma, O. Alfarraj, A. Tolba, and J. Wang, "A Dual Encoder Crack Segmentation Network With Haar Wavelet-Based High–Low Frequency Attention," *Expert Systems With Applications* 256 (2024): 124950.

60. X. Hang, X. Zhu, X. Gao, Y. Wang, and L. Liu, "Study on Crack Monitoring Method of Wind Turbine Blade Based on AI Model: Integration of Classification, Detection, Segmentation and Fault Level Evaluation," *Renewable Energy* 224 (2024): 120152.

61. C. Wang, Y. Zhang, and Z. Zhong, "Fault Diagnosis for Diesel Valve Trains Based on Time–Frequency Images," *Mechanical Systems and Signal Processing* 22, no. 8 (2008): 1981–1993.

62. S. J. Loutridis, "Instantaneous Energy Density as a Feature for Gear Fault Detection," *Mechanical Systems and Signal Processing* 20, no. 5 (2006): 1239–1253.

63. P. M. C. Monson, P. O. Conceição Junior, F. R. Lofrano Dotto, P. R. Aguiar, A. R. Rodrigues, and G. A. David, "Structural Damage Classification in Composite Materials Using the Wigner–Ville Distribution and Convolutional Neural Networks," *Materials Letters* 369 (2024): 136734.

64. J.-D. Wu and P.-H. Chiang, "Application of Wigner–Ville Distribution and Probability Neural Network for Scooter Engine Fault Diagnosis," *Expert Systems With Applications* 36, no. 2 (2009): 2187–2199.

65. A. Katunin, "Damage Identification and Quantification in Beams Using Wigner–Ville Distribution," *Sensors* 20, no. 22 (2020): 6638.

66. X. Li, Y. Xiao, H. Guo, and J. Zhang, "A BIM Based Approach for Structural Health Monitoring of Bridges," *KSCE Journal of Civil Engineering* 26, no. 1 (2022): 155–165.

67. J.-D. Wu and C.-K. Huang, "An Engine Fault Diagnosis System Using Intake Manifold Pressure Signal and Wigner–Ville Distribution Technique," *Expert Systems With Applications* 38, no. 1 (2011): 536–544.

68. D. Dai and Q. He, "Structure Damage Localization With Ultrasonic Guided Waves Based on a Time–Frequency Method," *Signal Processing* 96 (2014): 21–28.

69. Y. Liu, X. Hong, and B. Zhang, "Contact Delamination Detection of Anisotropic Composite Plates Using Non-Elliptical Probability Imaging of Nonlinear Ultrasonic Guided Waves," *Structural Health Monitoring* 22, no. 1 (2023): 276–295.

70. M. Luo, Y. Guo, Z. Su, et al., "Defect Quantification Evaluation of a Rolling Element Bearing Based on Physical Modelling and Instantaneous Vibration Energy Investigation," *Journal of Sound and Vibration* 600 (2025): 118875.

71. C. J. Stander, P. S. Heyns, and W. Schoombie, "Using Vibration Monitoring for Local Fault Detection on Gears Operating Under Fluctuating Load Conditions," *Mechanical Systems and Signal Processing* 16, no. 6 (2002): 1005–1024.

72. M. S. Yousefabad, M. H. Sadeghi, M. M. Ettefagh, Z. Mousavi, M. Bayat, and W. Q. Feng, "Detecting Different Damages by Smoothed Pseudo Wigner Ville Distribution and Convolution Neural Networks Under Different Loads: Crack and Scour Damages in Offshore Monopile," *Ocean Engineering* 343 (2026): 123363.